Application of Selective Laser Melting (SLM) for hybrid aerospace structures

Alex T. T. Nguyen[1,2,*], Milan Brandt[2], Adrian C. Orifici[1] and Stefanie Feih[1,3]

[1] *School of Aerospace, Mechanical and Manufacturing Engineering, RMIT University, PO Box 71, Bundoora, VIC 3083, Australia.*
[2] *Advanced Manufacturing Precinct, RMIT University, GPO Box 2476, Melbourne, Australia, 3001*
[3] *Joining Technology Group, Singapore Institute of Manufacturing Technology (SIMTech), Singapore 638075, Singapore*

[*] *Email: s3161514@student.rmit.edu.au*

Abstract: The study investigates the adhesion properties of SLM manufactured Titanium (Ti-6Al-4V) alloy surfaces for metal-metal and metal-composite hybrid joints using Mode I Double Cantilever Beam (DCB) specimens. The results indicate that the inherent micro-topology of the SLM surface is able to maximise the bonding potential of the adhesive. With the introduction of additional macro-surface features, the crack path is deflected from a straight mode I path and follows the design of the surface features. Selected macro-features were found to increase the fracture toughness by up to 50%. Finite element analysis indicates that the rise in fracture toughness is due to two factors: 1) the increase in the effective crack path length and 2) a shift from mode I to mode II crack growth.

Introduction

The use of composite materials, and especially carbon fibre-reinforced polymer (CFRP) composites, is increasing rapidly in the aerospace industry. Integrating composite materials with metal alloys can achieve hybrid structures with higher strength-to-weight ratio, longer inspection cycles and hence lower maintenance costs for modern aircraft. However, the connections between dissimilar materials are problematic due to stress concentrations, mismatch in thermal expansion and resulting fatigue issues [1,2]. One common joining method for hybrid structures is adhesive bonding which requires surface treatments (e.g. thermal, chemical, mechanical, laser or plasma) to ensure high strength and durability. These processes are lengthy and costly, particularly for titanium alloys.

Recently, additive manufacturing technology such as Selective Laser Melting (SLM) has seen increased application due to the enhanced design freedom and speed of manufacture. The surface topology created by the SLM process is unique due to the features of partially melted powder particles and results in an inherent significant roughness (10 µm to 15 µm), which is larger than the roughness achieved by advanced surface treatment methods for machined titanium surfaces (1 µm to 6 µm). Experimental investigation performed by Critchlow and Brewis [3] and Harris & Beevers [4] reported no correlation between surface roughness and adhesion properties, as the surface topology is an important factor that dictates the bond performance. It is, therefore, postulated that SLM component surfaces can be readily used for adhesion application with minimal additional cleaning and abrasive treatments.

Furthermore, using SLM technology, various forms of macro-features can be introduced on the adherend surface to improve joint performance. Numerical studies performed by Li et al. [5], Zavattieri et al. [6], Zhao et al. [7] and Zheng et al. [8] showed that the joint fracture toughness as well as strength can be increased by deflecting a straight crack path through interfering features, which is a bio-inspired concept. However, with the current manufacturing capabilities, the only macro-surface features that have so far been experimentally studied are carved out grooves using milling techniques. Da Silva et al. [9], Gao et al. [10], Kim et al. [11] and Lee et al. [12] reported that the macro surface features did not have a noticeable effect on the joint performance, but it is important to emphasise that crack deflection was not actually observed for these studies. Taking advantage of the SLM manufacturing flexibility to print virtually unlimited designs, various configurations of macro-surface features can be optimised to achieve maximum crack deflection.

This study investigates the adhesion properties of SLM manufactured titanium alloy (Ti-6Al-4V) surfaces. Mode I static fracture toughness tests are performed to establish the effect of SLM micro-roughness and macro-features on fracture toughness and hence adhesion strength. The SLM

titanium substrate is bonded to: 1) another SLM titanium substrate using FM300-2K adhesive; 2) a CFRP composite material (VTM-264) by co-curing. The fracture toughness of the Ti-Ti joints of as-built SLM components is compared with the machined titanium surface with grit-blasting surface treatment reported by Brack and Rider [13] and Donough et al. [14]. For the Ti-CFRP composite joint, the fracture toughness is compared to a CFRP-CFRP joint which was studied by Donough et al. [14] and Pingkarawat & Mouritz [15]. For the hybrid joint, the macro-surface features were found to increase the fracture toughness significantly. A numerical model was developed to determine the reason for the improved bonding strength of joints with macro-surface features.

Material and Methods

The titanium specimens were manufactured with a SLM250HL machine (SLM Solutions, Germany) within a build chamber of 250 mm × 250 mm × 350 mm. Prior to printing, the chamber is filled with Argon gas to avoid oxidation of the component during the manufacturing process. The chamber is pre-heated to 200°C to minimise the residual stresses during manufacturing. The adherends are printed with a layer thickness of 30 µm using a YLR-Fibre-Laser at 400 W. The process parameters are listed in Table 1. With these parameters, the SLM process is able to produce Titanium parts with a low porosity level of less than 0.3%.

Table 1: SLM process parameters

Laser	Layer	Scan	Energy	Hatch	Hatch	Spot Size	Chamber
175 W	30 µm	710 mm/s	68.5 J/mm^3	Checker-board	120 µm	80 µm	200°C

In order to avoid residual stresses and resulting plastic deformation of the specimens, long slender components are placed vertically on the build platform as shown in Figure 1 and at a 10° angle as shown in Figure 2. Four different surface configurations of inward and outward facing features (dimples and grooves) were introduced in order to study the effect of various macro-features on the joint performance. The characteristics of each configuration are illustrated in Figure 3. The out-of-plane height for each surface feature was set to 200 µm, which is in the order of one composite ply thickness.

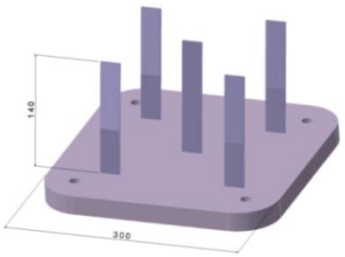

Figure 1: Build orientation (dimensions in mm)

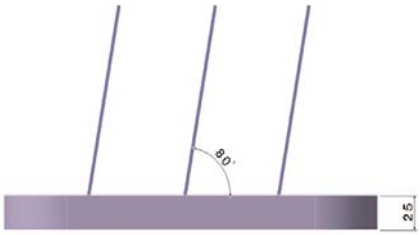

Figure 2: Build angle (dimensions in mm)

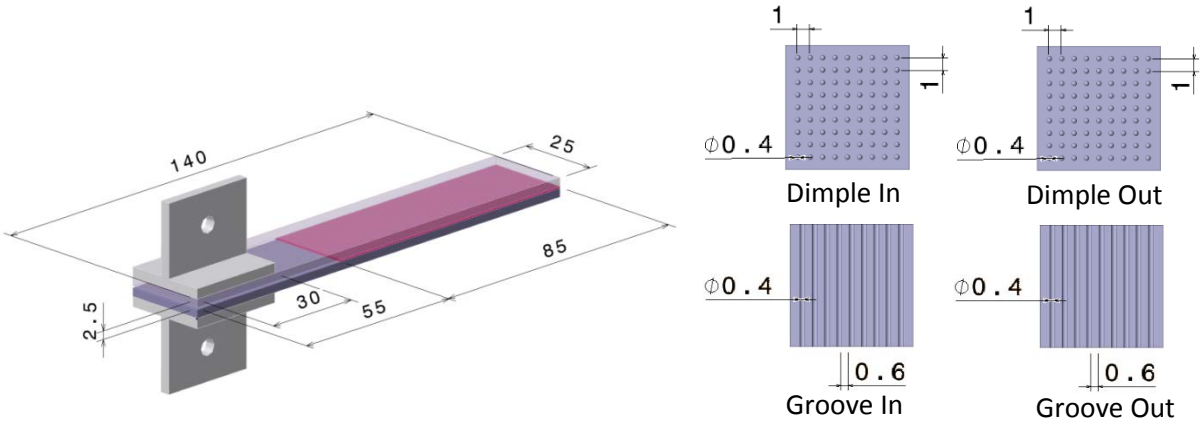

Figure 3: Mode I fracture test specimen (dimensions in mm)

The titanium adherends were joined with either another titanium adherend using FM300-2K adhesive or through co-curing with composite laminates made from T700 carbon/epoxy unidirectional prepreg plies (VTM264, Advanced Composites Group). Both curing processes took place in the autoclave according to manufacturer recommendations for the film adhesive and composite material. The dimensions of the mode I fracture specimens are indicated in Figure 3. For the Ti-composite hybrid joint, the bending stiffness between the dissimilar substrates was kept the same using Equation 1. The composite material was a 0° lay-up to match the titanium stiffness as closely as possible. Using material properties from Table 2, the thickness of the CFRP composite is 2.45 mm, which is equivalent to 11 plies. Two specimens were tested for each joint configuration with low scatter in results.

$$E_1 I_1 = E_2 I_2 \qquad \textbf{Equation 1}$$

Table 2: Material properties of VTM264, FM300-2K and Ti-6Al-4V

VTM264		**FM300-2K**		**Ti-6Al-4V**	
E_{11} (MPa)	117000	E (MPa)	2400	E (MPa)	110000
E_{22} (MPa)	9510	G (MPa)	840	G (MPa)	42500
E_{33} (MPa)	9510	ν	0.4	ν	0.32
G_{12} (MPa)	5900	X_T (MPa)	94.2	t (mm)	2.5
G_{12} (MPa)	5900	S_{12} (MPa)	54.4		
G_{23} (MPa)	3300	Y_e	0.055		
ν_{12}	0.32	Y_p	0.58		
X_T (MPa)	2459	G_{Ic}(KJ/m^2)	1.3		
Z_T (MPa)	48	G_{IIc} KJ/m^2)	5		
S_{12} (MPa)	88	t (mm)	0.2		
t (mm)	0.22				

The Mode I interlaminar fracture toughness (G_{Ic}) was determined by applying a monotonically increasing opening displacement at a rate of 2mm/min to the pre-cracked end of the Double Cantilever Beam (DCB) specimen. The crack length was measured using a travelling optical microscope. The Mode I interlaminar fracture toughness was calculated using modified beam theory:

$$G_{Ic} = \frac{3P\delta}{2b(a + \Delta a)} \qquad \textbf{Equation 2}$$

where P is the applied load, δ is the opening displacement, b is the width of DCB specimen, a is the crack length and Δa is a correction factor that is determined from compliance.

Result and Discussion

Titanium-Titanium Joint

Figure 4 and Figure 5 show the load versus displacement graphs and resulting fracture toughness according to Eq. (2) of the adhesively bonded Ti-Ti joints. Comparing the fracture toughness between plain surface specimens and the grit-blasted surface specimens indicates that there is no statistical difference between the two results. This suggests that the inherent micro surface features of the SLM surface are able to maximise the adhesion potential of FM300-2K adhesive without additional costly surface treatments. This is due to the surface characteristics of the SLM Titanium adherend. Figure 6 shows a typical SLM surface with an average surface roughness of 12 µm. This surface consists of a large amount of partially melted particles with an approximate diameter of 40 µm to 45 µm as shown in Figure 7. The topology of this surface is similar to the resulting topology for the advanced surface pre-treatment method as shown in Figure 8. The uniform ridges on the SLM surface essentially provide better wettability thus allowing full contact between the adhesive and the adherend. Moreover, these surface features also increase the overall contact area along with mechanical interlocking mechanism present to maximise the bonding ability of the adhesive. All specimens failed cohesively which

indicates that the interfacial strength between the adhesive and the adherend is higher than the strength of the adhesive itself. This type of failure is highly desirable for adhesive bonded joints.

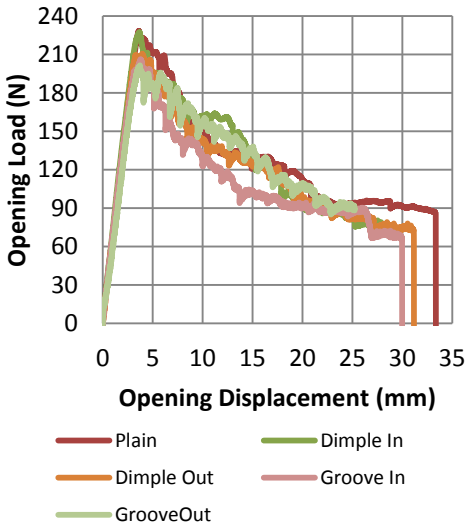

Figure 4: Opening load versus displacement for the Ti-Ti joint

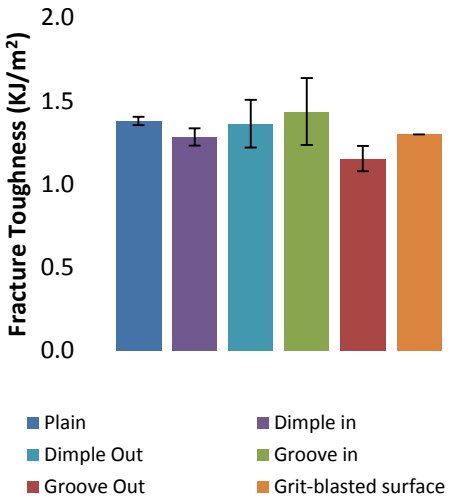

Figure 5: Fracture toughness for the Ti-Ti joint

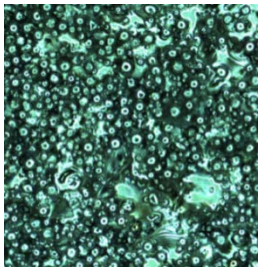

Figure 6: Surface characteristic of SLM component

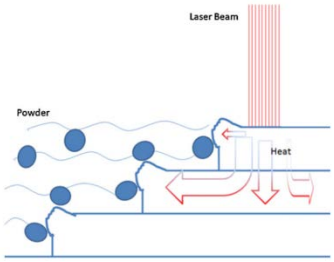

Figure 7: Partially melted particle on SLM surface (adopted from Strano et al. [16])

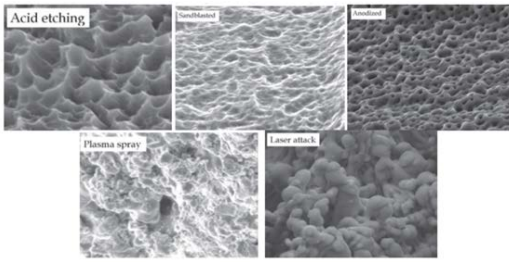

Figure 8: Surface characteristic of various advanced surface treatment (adopted from Elias [17])

When macro surface features were introduced, the peak load between all four configurations remained unchanged and varied between 200N-230N. In terms of fracture toughness, the values are statistically similar for all specimens and range between 1.2 kJ/m^2 to 1.4 kJ/m^2, a value which is equal to the mode I fracture toughness of the resin (Table 2). During the crack propagation process, the crack grew in the middle of the adhesive layer and there was no sign of crack deflection. Inspecting the fracture surface in Figure 9, all specimens failed cohesively along the adhesive carrier cloth, and there was no sign of deflection around the macro surface features. The result suggests that the size of these macro surface features was not effective at deflecting the crack for a Ti-Ti joint due to the relatively low toughness of the film adhesive.

(a) (b)

Figure 9: (a) Crack propagation in the middle of the adhesive layer and (b) top (left) and bottom(right) adherend surface from a cohesively failed surface

Titanium-CFRP Joint

The load-displacement graphs and resulting steady-state fracture toughness values for the SLM Titanium substrate co-cured with CFRP are shown in Figure 10 and Figure 11. The fracture toughness of the hybrid joint exceeds the fracture toughness for CFRP-CFRP joint specimens for all test cases as indicated in Figure 11 [7, 15]. Upon crack growth, the starter crack immediately deflects into the first zero ply of the CFRP composite. The fracture surface shows a large amount of fibre bridging resulting from the 0° ply interfaces during the crack growth process as shown in Figure 12 and Figure 13. A similar trend is observed for all specimens. The results indicate that the strength of the interface between SLM surface and composite material - regardless of surface features - is higher than the interlaminar strength of the VTM264 composite (1.0 kJ/m^2), therefore leading to the crack jump phenomenon.

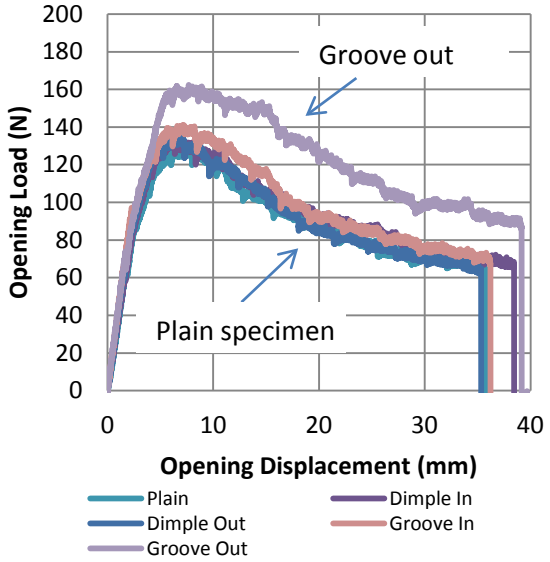

Figure 10: Opening load versus displacement for the Ti-CFRP joint

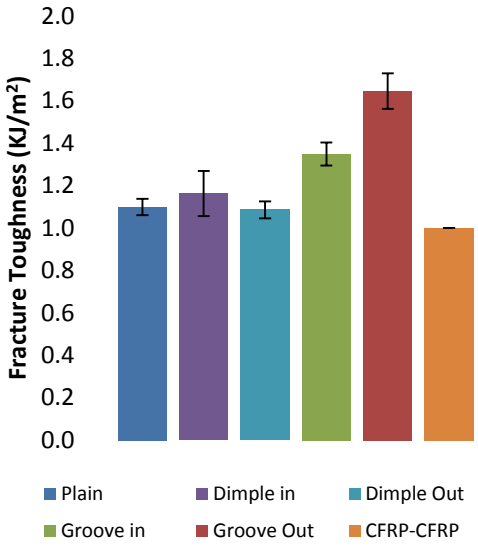

Figure 11: Fracture toughness of the Ti-CFRP joint

In terms of macro features, the 'dimpled' specimens did not show any visible effect on opening load and fracture toughness as compared to the plain specimen due to their inability to change the crack path. However, a significant difference was observed for the test cases with 'groove out' and 'groove in' features. These specimen reached a significantly higher maximum load of up to 160 N (compared to 125-130N for the other test cases). This difference in maximum load between the 'groove' macro feature and the plain specimens results in an almost 50% increase in fracture toughness. The crack path is clearly observed to follow around the 'groove' feature within the first composite ply (see Figure 13). The numerical analysis in the next section quantifies the failure mechanism that is responsible for the increase in fracture toughness.

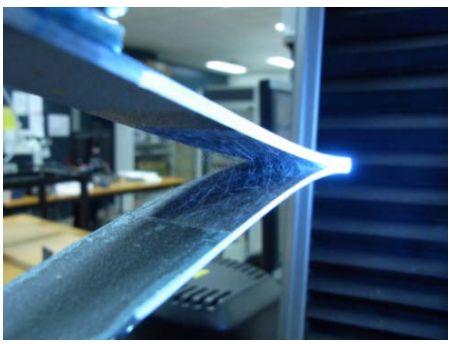

Figure 12: Crack deflection from initial flaw into composite material

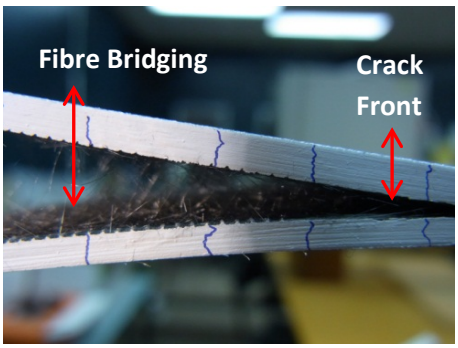

Figure 13: Large amount of fibre bridging behind crack front and "groove out" surface feature

Numerical modelling

During the crack-propagation process, a high level of bridging at the laminate interface was observed. In order to simulate this additional damage mechanism, the procedure introduced by Dávila et al. [18] was adopted. In this procedure, two cohesive elements [19] with different properties are superposed at the same location. Essentially, the first cohesive element with high strength and low toughness is used to represent the resin crack front while the second cohesive element with low strength and high toughness is used to represent the fibre bridging mechanism.

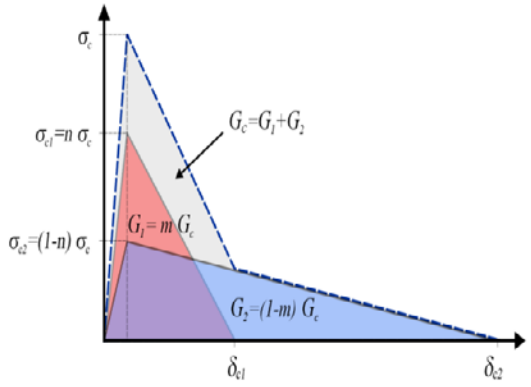

Figure 14: Superposed cohesive element with two bi-linear law [18]

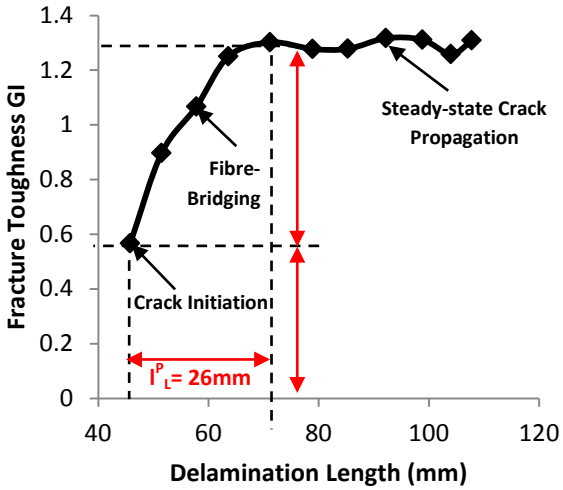

Figure 15: Idealidation of R-curve into 3 separate segments

The R-curve in Figure 15 can be idealised into 3 separate segments: the crack initiation, the fibre bridging and the steady-state crack propagation. The resin fracture is accurately described by the bi-linear law due to the brittle fracture process. The second bi-linear law for fibre bridging was further modified in this work through an exponential law as described by Feih et al. [20] to capture the experimental data trend more accurately. In this case, the damage evolution is of exponential shape and influenced by a non-dimensional parameter α [19]:

$$D = 1 - \left\{\frac{\delta_m^0}{\delta_m^{max}}\right\}\left\{1 - \frac{1 - \exp(-\alpha\left(\frac{\delta_m^{max} - \delta_m^0}{\delta_m^f - \delta_m^0}\right))}{1 - \exp(-\alpha)}\right\} \qquad \textbf{Equation 3}$$

Material parameters for the cohesive laws were determined based on literature and simulation of mode I and mode II tests of the CFRP-CFRP interlaminar strength. The numerical analysis was performed in Abaqus/Standard 6.12 [19]. The parameters that are used to describe the cohesive laws for delamination and fibre bridging are summarised in Table 3.

Table 3: Cohesive parameters of superposed elements

Damage Mechanism	Strength σ (MPa)	Fracture toughness G_{IC} (kJ/m^2)	Fracture toughness G_{IIC}(kJ/m^2)	Penalty Stiffness K(MPa)	Opening Displacement δ(mm)	Exponential alpha α
Delamination	44.35	0.21	2.2	10^6	-	-
Fibre Bridging	2.1	-	-	10^6	4	10

For the “groove out” specimen, the grooves were explicitly modelled, and the crack path was specified to follow around the grooves as oberserved in the experiment (see Figure 16). A resin-rich area around the surface features was included in the model. Following the new crack path, the overall total crack length is increased by 55%, which is signficant considering the small out-of-plane height of the surface features. Once the crack starts to deviate from the straight path, the crack growth mode

changes from a pure mode I to a mixed mode with mode II contribution. While the fibre bridging is not considered to contribute to mode II crack growth resistance, the fracture toughness of epoxy resins under mode II is generally significantly larger than under mode I (see Table 3).

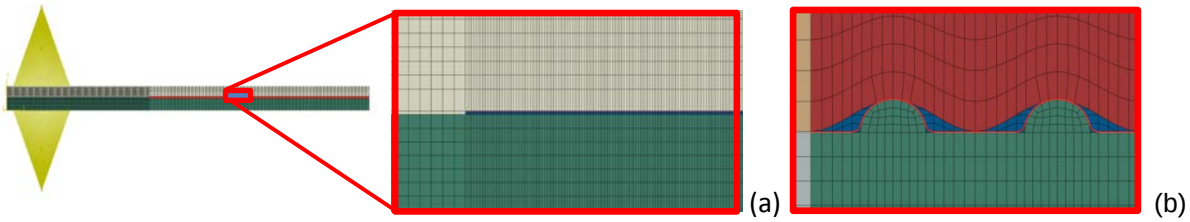

Figure 16: Crack path of the groove out macro feature specimen. (a) Plain (b) Groove out.

Figure 17 and Figure 18 compare the the load-displacement curve and the R-curve of the numerical model with the experimental data. The results indicate that the modelling approach is able to accurately capture both the crack propagation as well as fibre bridging damage mechanism both in terms of maximum opening load with opening displacement and the increase in the fracture toughness with crack length for both plain specimens and specimens with groove surface features. The increase in load and steady-state fracture toughness is captured accurately. The contribution of fibre bridging to the fracture toughness is shown to be significant and much larger than the fracture toughness at crack initiation. The fibre bridging zone is fully developed once the crack has extended by roughly 20 mm.

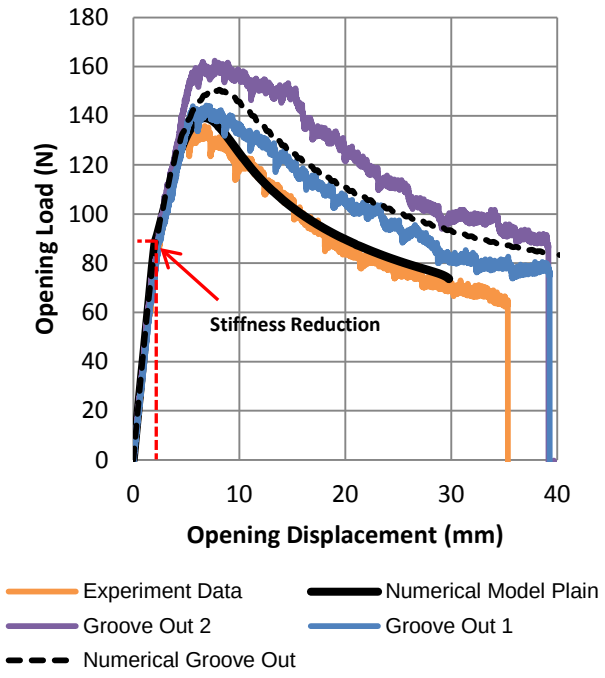

Figure 17: Load versus displacement of numerical and experimental data

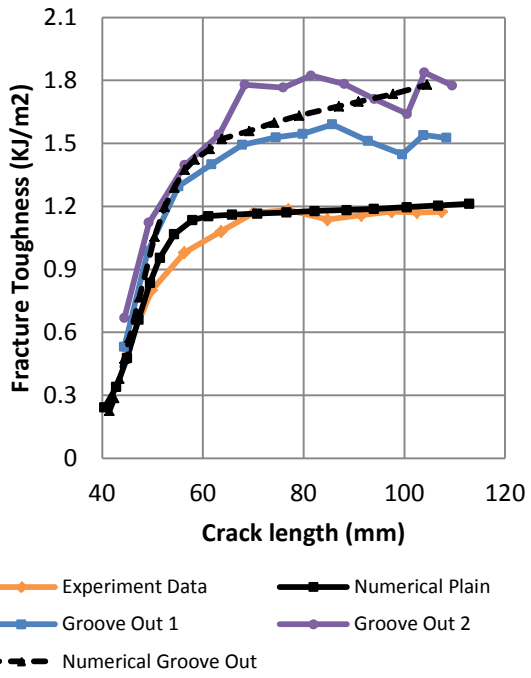

Figure 18: Fracture toughness of numerical and experimental data

To establish the reasons for the increased load (and fracture toughness) for the 'groove out' specimens, the analysis was run in two separate stages: (1) just mode I parameters but considering the deflected crack path and (2) considering both mode II parameters and the deflected crack path. For the first numerical analysis, the peak load remained at approximately 140N and the fracture toughness increase by approximately 27%. When the mode II fracture toughness for the resin was introduced, the peak load increased to 150N and the fracture toughness increased by approximately 50%. Based on this analysis, both factors of crack length increase and mode II crack growth contribute equally to the enhancement of fracture toughness through crack deflection. Future work will focus on the optimisation of the surface macro-features to maximise the deflected crack path and mode II crack growth contribution.

Conclusion

An investigation on the adhesion properties of SLM manufactured titanium alloy surfaces using Mode I fracture toughness tests was performed. The fracture toughness results indicated that the adhesion strength of SLM titanium surfaces without any additional surface treatment is at least as good as that of the machined titanium surface with grit-blasting surface treatment. This result confirmed that the as-built surface characteristics of SLM components are able to provide an increased contact area and mechanical interlocking between adhesive and adherend, which in turn maximises the adhesion potential of the adhesive.

Furthermore, when the SLM surface is co-cured with a composite material, the crack front is deflected into the composite material (first / second ply interface), which emphasises that the interface strength of the hybrid structure is higher than the interlaminar composite strength.

When macro features are introduced, both the effective increase in crack length and the deflection from mode I to mode II crack growth are responsible for increasing the fracture toughness of the bonded joint by about 50%.

.

Reference

1. Baldan, A. (2012). Adhesion phenomena in bonded joints. International Journal of Adhesion and Adhesives, 38(0), 95-116.
2. Brockmann, W. (2009). Adhesive bonding : materials, applications and technology. Weinheim: Wiley-VCH.
3. Critchlow, G. W., & Brewis, D. M. (1995). Influence of surface macroroughness on the durability of epoxide-aluminium joints. International Journal of Adhesion and Adhesives, 15(3), 173-176.
4. Harris, A. F., & Beevers, A. (1999). The effects of grit-blasting on surface properties for adhesion. International Journal of Adhesion and Adhesives, 19(6), 445-452.
5. Li, B.-W., Zhao, H.-P., Qin, Q.-H., Feng, X.-Q., & Yu, S.-W. (2012). Numerical study on the effects of hierarchical wavy interface morphology on fracture toughness. Computational Materials Science, 57(0), 14-22.
6. Zavattieri, P. D., Hector Jr, L. G., & Bower, A. F. (2008). Cohesive zone simulations of crack growth along a rough interface between two elastic–plastic solids. Engineering Fracture Mechanics, 75(15), 4309-4332.
7. Zhao, H.-P., Wang, Y., Li, B.-W., & Feng, X.-Q. (2013). Improvement of the peeling strength of thin films by a bioinspired hierarchical interface. International Journal of Applied Mechanics, 05(02), 1350012
8. Zheng, X.-P., Cao, Y.-P., Li, B., Feng, X.-Q., & Yu, S.-W. (2010). Surface wrinkling of nanostructured thin films on a compliant substrate. Computational Materials Science, 49(4), 767-772.
9. Da Silva, L. F. M., Ferreira, N. M. A. J., Richter-Trummer, V., & Marques, E. A. S. (2010). Effect of grooves on the strength of adhesively bonded joints. International Journal of Adhesion and Adhesives, 30(8), 735-743.
10. Gao, H. T., Yang, X., Huang, P., & Xu, K. W. (2013). Enhancement mechanism of super fine machining pattern on mechanical property of adhesion interface of Al alloy. Physics Procedia, 50(0), 288-292.
11. Kim, W.-S., Yun, I.-H., Lee, J.-J., & Jung, H.-T. (2010). Evaluation of mechanical interlock effect on adhesion strength of polymer–metal interfaces using micro-patterned surface topography. International Journal of Adhesion and Adhesives, 30(6), 408-417.
12. Lee, M. J., Kim, W. S., Jang, C. J., Kim, K. H., Cho, T. M., Lee, B. C., & Lee, J. J. (2011). Analysis and Simulation of the Failure Characteristic of a Single Leg Bending Joint with a Micro-Patterned Surface. The Journal of Adhesion, 87(7-8), 826-841.
13. Brack, N., & Rider, A. N. (2014). The influence of mechanical and chemical treatments on the environmental resistance of epoxy adhesive bonds to titanium. International Journal of Adhesion and Adhesives, 48, 20-27.
14. Donough, M. J., Gunnion, A. J., Orifici, A. C., & Wang, C. H. (2012). Critical assessment of failure criteria for adhesively bonded composite repair design. International Congress of The Aeronautical Sciences, Brisbane.
15. Pingkarawat, K., & Mouritz, A. P. (2014). Improving the mode I delamination fatigue resistance of composites using z-pins. Composites Science and Technology, 92, 70-76.
16. Strano, G., Hao, L., Everson, R. M., & Evans, K. E. (2013). Surface roughness analysis, modelling and prediction in selective laser melting. Journal of Materials Processing Technology, 213(4), 589-597.
17. Elias, C. N. "Factors affecting the success of dental implants [Internet]." Rijeka: InTech (2014).
18. Dávila, C., Rose, C., & Camanho, P. (2009). A procedure for superposing linear cohesive laws to represent multiple damage mechanisms in the fracture of composites. International Journal of Fracture, 158(2), 211-223.
19. ABAQUS Version 6.12 Documentation (2012), Dassault Systémes Simulia Corporation.
20. Feih, S., Wei, J., Kingshott, P., & Sørensen, B. F. (2005). The influence of fibre sizing on the strength and fracture toughness of glass fibre composites. Composites Part A: Applied Science and Manufacturing, 36(2), 245-255